

RESEARCH ARTICLE

Microstructural examination of interactions between chromia-based refractory and nuclear glass in a melter

Natalie J. Smith-Gray¹ | John M. Bussey² | John S. McCloy^{1,2}

¹Materials Science and Engineering Program, Washington State University, Pullman, Washington, USA

²School of Mechanical and Materials Engineering, Washington State University, Pullman, Washington, USA

Correspondence

John McCloy, Materials Science and Engineering Program, Washington State University, Pullman, WA, USA.

Email: john.mccloy@wsu.edu

Abstract

This study shows the effects of nuclear waste glass production on Monofrax K-3 refractory corrosion. A continuously fed research-scale melter containing an Fe- and Ni-rich simulated nuclear waste feed with borosilicate glass-forming chemicals was cyclically melted at 1150°C and idled at 1050°C for a total of 11 weeks. Chemical maps using scanning electron microscopy show the interactions between the quenched melt and the refractory. Nanoscale X-ray-computed tomography was used for a three-dimensional visualization of certain parts of the interface. Unreacted K-3 consists of primarily corundum (Al,Cr)₂O₃ and spinel (Fe²⁺,Mg)(Al,Cr)₂O₄ interlocking crystalline phases. Some of the Cr from the refractory interacts with the Ni and Fe from the melt to form a reaction layer comprising (Ni,Fe²⁺)(Cr,Fe³⁺)₂O₄ spinel crystals. Simultaneously, melt components (Na,Si) infiltrate into the refractory. This interaction proceeds at the expense of the integrity of the refractory structure. Intact refractory grains (e.g., (Al,Cr)₂O₃) as well as the reaction layer itself can lose mechanical integrity and spall off into the melt, especially near the top of the melter. As the reaction layer can be a protective boundary for the refractory against further melt infiltration, a reduction in the reaction layer thickness allows an increase in refractory corrosion.

KEYWORDS

corrosion, nuclear waste vitrification, refractory, research-scale melter

1 | INTRODUCTION

Refractory corrosion results from a combination of chemical (corrosive) wear, physical (erosive) wear, operational conditions, and refractory build (type, arrangement, etc.).^{1–4} Refractory corrosion, due to interaction with glass melts at high temperature, results in the required replacement of refractory components or even the whole melter assembly. For typical commercial continuous melters or nuclear waste glass melters, this period is

typically 5–20 years and is sometimes known as the “campaign lifetime.”^{5–7} For a typical high Cr₂O₃ refractory, corrosion can also be a contributor to the formation of spinel crystals.^{8–10} These spinels can form in nuclear waste glass compositions simply due to the composition and solubility of these metals and the crystal liquidus temperature, without exposure to transition-metal-containing refractories.^{11–13} Spinel crystals do not decrease borosilicate glass aqueous chemical durability; however, upon accumulation, these crystals may clog the melter riser and

This is an open access article under the terms of the [Creative Commons Attribution](https://creativecommons.org/licenses/by/4.0/) License, which permits use, distribution and reproduction in any medium, provided the original work is properly cited.

© 2022 The Authors. *Journal of the American Ceramic Society* published by Wiley Periodicals LLC on behalf of American Ceramic Society.

pour spout, preventing the glass from being poured into canisters.¹⁴ Understanding the various corrosion mechanisms is important in developing methods to reduce the corrosion. Reducing corrosion within a melter could save material, money, and time.

1.1 | Physical (erosive) wear

There are multiple erosive-driven mechanisms, including natural convection that occurs when there is a density difference within a melt. Corrosion will cause refractory to dissolve into the melt, which then makes that section of the melt denser.^{1,3} As the denser melt sinks, it can interact with vertical refractory walls leaving a “trail” of dissolved particles.^{1,3} This in turn may cause the melt to become less dense, which prompts it to rise to the surface. This process is also known as “density-promoted flow.”¹

Forced convection is another type of erosion that occurs when molten glass is agitated by mechanisms such as bubbling.^{1,3} Forced convection can cause materials to continuously be removed from the boundary layer, which in turn increases the refractory dissolution rate.^{1,3}

The greatest amount of refractory corrosion is generally the flux line corrosion.¹ The flux line is where the melt, air, and refractory meet; this corrosion is driven by surface energy, which is highly dependent on melt composition and slightly on temperature.¹ As refractory dissolution occurs, the density of the melt increases, which increases the surface energy.¹

1.2 | Chemical (corrosive) wear

Refractory degradation due to chemical corrosion from a glass composition arises from the system attempting to create an equilibrium between the refractory (the solute) and the glass melt (the solvent).¹ This process involves several important steps as outlined later. Diffusion occurs when ions from the melt penetrate within the refractory grains, along the grain boundaries, or into the refractory pores that can lead to dissolution.¹⁵ At the same time, components from the refractory can dissolve into the melt. Several factors that contribute to the oxide dissolution rate include (I) the diffusion rate of refractory components into the glass melt, (II) solubility of the refractory elements in the melt, (III) mobility of the reacting species within the melt, and (IV) mobility of the dissolved refractory within the melt.¹ This mobility is related to the glass viscosity, and it has been shown that a lower viscosity can result in higher melt infiltration and thus greater corrosion.¹⁶

The most important aspect of melt–refractory interactions with Cr₂O₃-containing refractories, however, is

the formation of passivating intermediate layers of spinel crystals between the glass melt and the refractory. This phenomenon has been observed over many years for both nuclear waste glasses^{16,17} and for coal gasifiers.¹⁸ The process is essentially as follows: Spinel formation is a product of indirect dissolution, a heterogenous reaction that involves the counter-diffusion of ions between glass and refractory.^{19,20} Essentially a passivation layer (“reaction layer”) is formed where a high melting point transition metal spinel (i.e., AB₂O₄, where A and B are metals such as Al³⁺, Cr³⁺, Fe³⁺, Fe²⁺, Mg²⁺, Ni²⁺, and Zn²⁺) is created at the refractory–melt interface.

The process of diffusion, dissolution, and spinel formation contributes to the formation of this boundary or reaction layer. This layer forms when the rate of chemical reaction is faster than the removal of reaction products, creating an interface between the refractory and glass that is saturated with reaction products.^{1,4} In a stagnant melt, this would be considered a “Type III in situ” refractory surface by Lee et al.,²¹ in which the boundary layer may passivate the overall corrosion of the refractory. When forced convection occurs (i.e., melt stirring), the boundary layer is decreased and replaced by fresh melt, a process called direct dissolution.⁴ In nuclear waste glasses rich in iron and nickel oxide, NiFe₂O₄ (trevorite) spinels will typically form this boundary layer.²² In very high chrome refractories, such as those used in coal gasifiers in contact with iron-rich coal slags, FeAl₂O₄ (hercynite) and FeCr₂O₄ (chromite) are the typical spinel phases formed.¹⁸

1.3 | Spinel formation

Postmortem analysis of a failed Defense Waste Processing Facility nuclear waste glass melter lined with Monofrax K-3 refractory showed that Cr from the refractory did dissolve in the glass and influenced the spinel composition, which was found to be enriched in Cr.⁹ As K-3 refractory is mostly an (Mg,Cr) spinel solid solution, that is, (Fe²⁺,Mg)₂(Cr,Al)₂O₄, plus an (Al,Cr) oxide corundum phase (i.e., α-(Cr,Al)₂O₃), with some other minor components like zerovalent iron,¹⁷ spinel is already an important crystal phase in the starting refractory. The formation of the (Ni,Fe) spinel¹⁷ or (Zn,Fe) spinel¹⁶ involves, to an extent, the cation exchange of the spinel phase in the refractory brick itself, and the creation of new spinel crystals at the interface. Jantzen et al.^{9,17} have summarized a number of tests in different compositions and feeds and described the phenomena.

Spinel can also precipitate from nuclear waste glasses and will settle on the bottom of the melter.^{12,23} Accumulation rates of the spinel formation (which may or may not be due to refractory interaction) have been

modeled and shown to be more rapid with oxidizing feeds, by $\sim 2\text{--}3\times$, and will also be greater with mechanical stirring in the melt.⁹ Under various conditions, the spinel settling and potential plugging of the pour spot have been modeled.^{14,17}

Where crucible corrosion tests are used to evaluate refractories, corrosion by dissolution into the glass is often the predominant factor evaluated.^{17,24} However, this will be limited by low convection currents and thermal gradients. Bubbling in the crucible and feeding slurry can begin to simulate conditions of a production melter, but the dynamics of a melter cannot be completely simulated in crucible corrosion studies. For this reason, the evaluation of crucible corrosion results must carefully consider the conclusions and recommendations presented when a corrosion rate is discussed and expected to be applied to a melter design or when comparing results of past studies. Melter designers, and anyone evaluating refractories for melter construction, must be aware of all refractory failure modes and how each could challenge melter performance.

2 | MATERIALS AND METHODS

To illustrate the chemical reactions described before, sections of a research-scale melter (RSM) used at the Pacific Northwest National Laboratory were dissected and subjected to microstructural and chemical analysis using a scanning electron microscope (SEM) equipped with energy-dispersive spectroscopy (EDS). The purpose of the RSM test was to study spinel formation in the glass and its accumulation, so as to evaluate the susceptibility of the refractory riser (pour spout) to spinel plugging.¹⁴ The RSM itself is described therein, but briefly consisted of two layers of Monofrax K-3, whereas the slurry feed used was an Ni- and Fe-rich high-level waste simulated glass, known as AZ-101 waste simulant, designed to mimic the glass production of the waste from the Hanford Tank 241-AZ-101. The target glass composition has a complex composition,¹⁴ but is essentially a sodium borosilicate glass (17.81-wt% Na_2O , 7.63-wt% B_2O_3 , 38.47-wt% SiO_2) with some other components, the important ones for the analysis of the refractory interaction data being Fe_2O_3 (17.5 wt%), Al_2O_3 (7.84 wt%), NiO (1.50 wt%), Cr_2O_3 (0.16 wt%), and MgO (0.12 wt%). The complete target glass composition¹⁴ is provided within the Supporting Information section (Table S1). The melter inner diameter was reported¹⁴ at 15.2 cm with a height of 14.0 cm, and the nominal glass melt depth was 10.5 cm. The experiment involved processing 509 kg of feed over a period of 11 weeks. The test cycled between 11 feeding/pouring and 11 idling periods, lasting 36 h and 4–7 days, respectively.¹⁴ During the

feeding/pouring periods, the targeted melt temperature was 1150°C and automatically controlled by a data acquisition control system; the idling periods were at a lower temperature of 1050°C.¹⁴ The diagram in Figure 1 shows the layout of the melter and the location of the dissected samples within this study. A study of the refractory interaction with the glass was not the purpose of the original RSM study,¹⁴ but some analysis of the refractory–melt interface was previously performed by Monofrax, the manufacturer of K-3 refractory.²²

A saw blade was used to cut the RSM fragments to extract several sample pieces to fit the SEM stage. Each sample was then oil polished down to 1- μm grit size and cleaned with deionized water and ethanol. A field emission SEM was used for imaging, EDS point scans, and the collection of EDS chemical maps. The operating voltage ranged between 20 and 25 kV, scan size ranged from 3 to 6 (relat, and the working distance was 5 mm for EDS scans and collection of chemical phase maps (CPMs).

Electron probe microanalysis (EPMA) was used for a chemical analysis of the solid glasses to assess batched versus actual compositions. A JEOL JXA-8500F field emission electron microprobe was used, equipped with five wavelength-dispersive X-ray spectrometers (WDS) operating at 15-keV accelerating voltage, 10-nA beam current, and 5- μm beam size. Probe for EPMA²⁵ was used to analyze the WDS data.

Nanoscale X-ray-computed tomography (nano-CT) was conducted to observe microstructural features from ~ 50 nm to 65 μm . Nano-CT measures X-ray attenuation from different angles, creating a three-dimensional (3D) model that generally distinguishes between phases with differences in atomic number (Z) and density. Nano-CT was conducted on the Zeiss Xradia 810 Ultra at the WSU Institute for Materials Research user facility. For nano-CT imaging, a small shard (~ 200 μm in the longest direction, ~ 10 μm thick) from the top of the RSM (the green box in Figure 1) was mounted on a sewing pin using UV-curing adhesive (Bondic). In order to contextualize the sample, a mosaic of 2D X-ray transmission projections was compiled using a 5.4 keV Cr K_α X-ray source, an X-ray detector with 128-nm sized pixels, and a Zernike phase contrast filter. Using the same X-ray source and detector, but without a contrast filter, 361 X-ray projections were captured while rotating the sample 140°, with a 90-s exposure, detector pixels binned in pairs, and a 65- μm field of view. XRM reconstructor (Zeiss) and Dragonfly software (Object Research Systems) were used to reconstruct the projections and visualize the resulting 3D model. In order to highlight phase differences, the X-ray attenuations were thresholded (desired range of X-ray attenuations selected) and false-color adjusted (grayscale values placed in chromatic order using a lookup table).

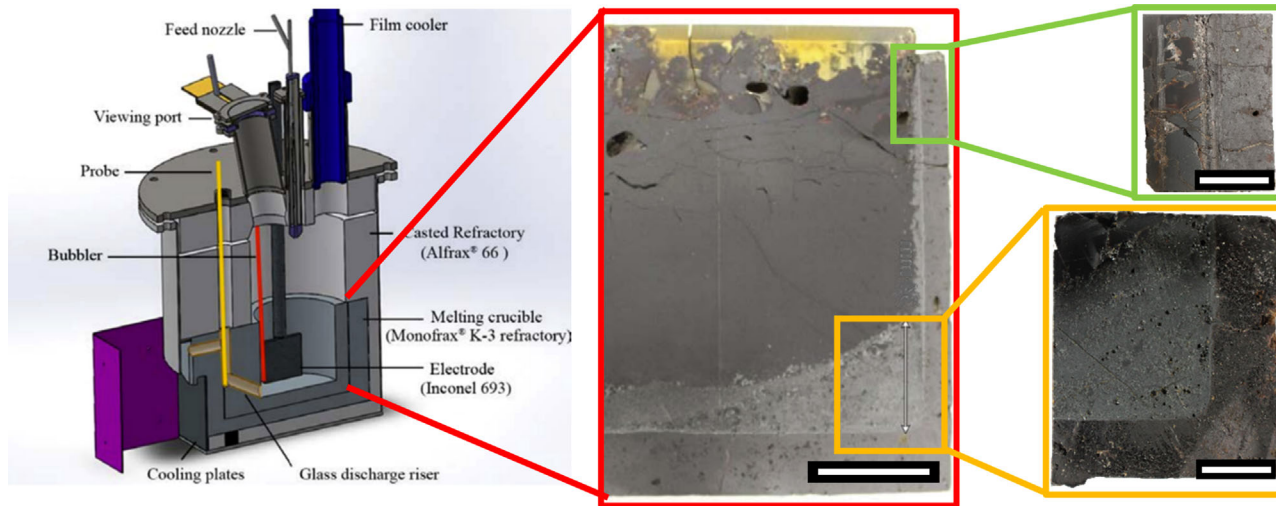


FIGURE 1 Diagram of the research-scale melter (left), an image cross-sectioned from the research-scale melter (RSM) with a scale bar of 3.4 cm (middle), and images of the samples used in this study with a scale bar of 1.27 cm. Partially modified from Ref. [14], used with permission courtesy of Battelle Memorial Institute

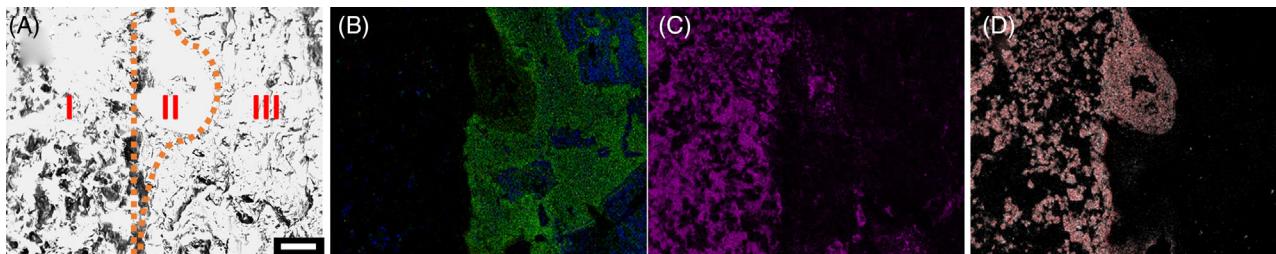


FIGURE 2 Chemical phase map located near the top of the research-scale melter (RSM) with a 100- μm scale. (A) Secondary electron (SE) image with three locations labeled (I) melt, (II) reaction layer, and (III) refractory along with lines indicating the approximate boundaries of each; (B) Cr represented as green and Al as blue; (C) Si as magenta; (D) Fe as gray and Ni as red, overlapped colors create the pink hue as shown.

3 | RESULTS

3.1 | Refractory and reaction layer

X-ray diffraction (XRD) analysis of Monofrax K-3 shows that it is comprised of two phases, mostly corundum $(\text{Al,Cr})_2\text{O}_3$ and spinel $(\text{Fe}^{2+},\text{Mg})(\text{Al,Cr})_2\text{O}_4$. No attempt was made to obtain precise stoichiometry from XRD. Beginning with a CPM collected near the top of the melter, Figure 2A shows several regions labeled the (I) melt region, (II) reaction layer, and (III) refractory. The section of refractory mostly contains Cr, Al, and Mg (Figure 2B), which is expected from both literature¹⁷ and XRD results. Some Al and Cr appear in clusters within the melt (Figure 2B), which will be discussed later.

A CPM collected at the melter wall deeper into the RSM is shown in Figure 3. Again the three regions of the (I) melt, (II) reaction layer, and (III) refractory are labeled in

Figure 3A. A large portion of Na, represented as magenta in Figure 3D, is present within the refractory region. By contrast, near the top of the RSM, there was limited Na within the refractory.

When the melt comes into contact with the refractory, ions exchange at the interface between the two materials and a reaction layer forms.¹ Thermodynamic assessment has shown that an NiCrFeO_4 spinel (idealized composition after reaction at the interface) is more stable than an MgAlCrO_4 spinel (nominal starting K-3 spinel composition), thus driving the reaction toward the interface spinel composition.⁹ Evidences of the NiCrFeO_4 spinels are seen throughout this study in both the reaction layer in region (II) of Figures 2 and 3, and floating within the melt indicated with arrows in Figures 6 and 7.

The thickness of the reaction layer varies throughout the RSM as shown in Figure S1. Near the top of the RSM, the reaction layer is thin due to forced melt convection, while

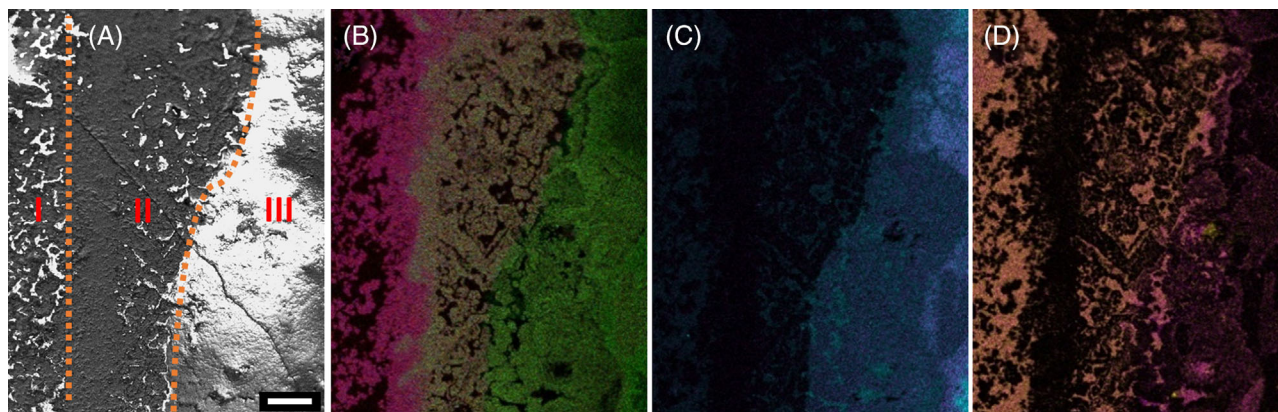


FIGURE 3 Corrosion of research-scale melter (RSM) wall with a 100- μm scale. (A) secondary electron (SE) image with three locations labeled (I) melt, (II) reaction layer, and (III) refractory along with lines indicating the approximate boundaries of each; (B) Fe is represented in red, Ni in blue, and Cr in green, with the reaction layer being a yellow hue due to the combination of all three colors; (C) Al in blue and Mg in green; (D) Si in yellow and Na in magenta, overlapped colors create orange.

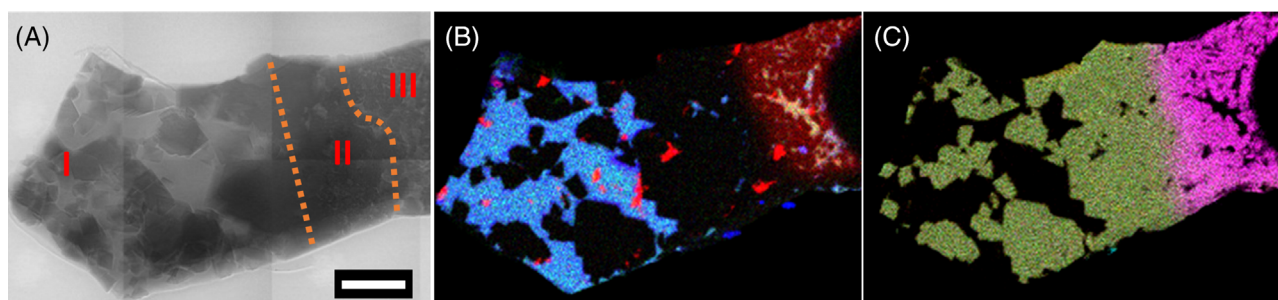


FIGURE 4 (A) Mosaic of nanoscale X-ray-computed tomography (nano-CT) projections of a top piece of the research-scale melter (RSM) with a 50- μm scale bar. Three regions labeled (I) melt, (II) reaction layer, and (III) refractory along with lines indicating the approximate boundaries of each; (B) Si is represented as blue, Na as green, and Al as red; (C) Fe is represented as yellow, Ni as cyan, and Cr as magenta

further down into the melter, which is impacted less by melt convection, there is a thicker reaction layer. At the base of the RSM, spinels formed from transition metals present in the glass plus ions released into the glass from the refractory corrosion, in addition to spinel phases that have reacted and spalled off the refractory, settle on the reaction layer at the base forming a thick layer of spinels. Matyáš et al.¹⁴ found that crystals were present in the glass before idling is initiated, which creates nucleation sites. The larger crystals would slowly settle at the bottom of the RSM, whereas crystals smaller than 10 μm would remain suspended within the glass.¹⁴

A small shard from the top of the RSM was removed for nano-CT imaging and chemical phase mapping (Figure 4). The three regions (I) melt, (II) reaction layer, and (III) refractory are labeled in Figure 4A. In Figure 4B, Si is represented as blue, Na as green, and Al as red. The Al is enriched within the refractory region (III) and is found in clusters throughout the melt, likely refractory that has spalled into the melt. The refractory region, while mostly

red due to Al, has regions with a green–blue hue due to the presence of the Na and Si. This is indicative of glass infiltration into the refractory. In Figure 4C, Fe is represented as yellow, Ni as cyan, and Cr as magenta. The refractory region (III) is enriched with Cr (and Al) with a little indication of the presence of Fe and Ni indicating that this area is predominately corundum refractory. The melt region (I) and the reaction layer (II) are a dull green color, which is the color combination of Fe (yellow), Ni (cyan), and Cr (magenta).

The refractory region was further investigated with nano-CT imaging, focusing specifically in the area within the orange box in Figure 5A. The blue coloration in Figure 5 is indicative of a phase with a relatively low average atomic number (Z) and density in comparison to the green coloration, which is indicative of a phase with relatively high Z and density. The high- Z region is enriched with Cr, Fe, and Ni, as shown in Figure 4C. The low- Z region is enriched with Na, Si, and Al, as shown in Figure 4B. The Na and Si are foreign to the refractory, a result of glass

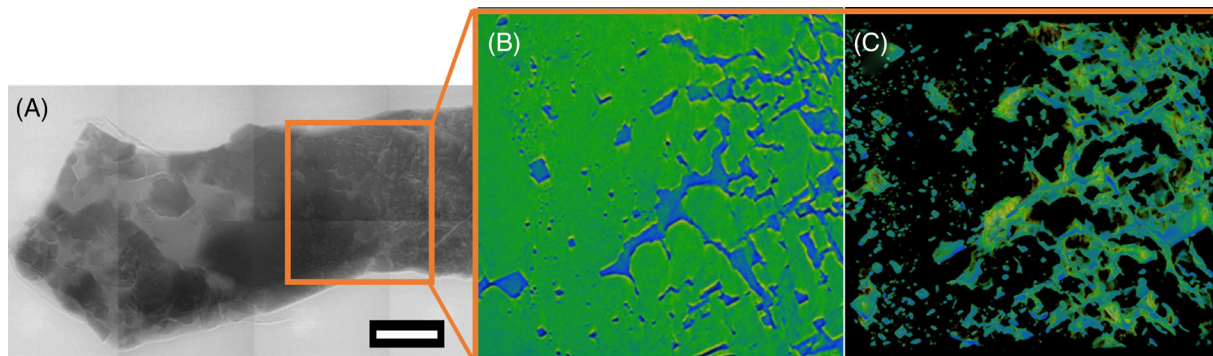


FIGURE 5 (A) Mosaic of nanoscale X-ray-computed tomography (nano-CT) projections of a top piece of the research-scale melter (RSM) with a 50- μm scale bar. The orange box indicates the location of the two-dimensional (2D) nano-CT image and video (B) that shows two primary phases, one with comparatively low atomic number (Z) and density in blue and one with comparatively high Z and density in green. Part (C) shows an image of a 3D nano-CT rendering of the orange box marked in (A), thresholded to highlight the lower atomic number (Z) and density regions. The horizontal field of view for (B) and (C) is $\sim 70 \mu\text{m}$.

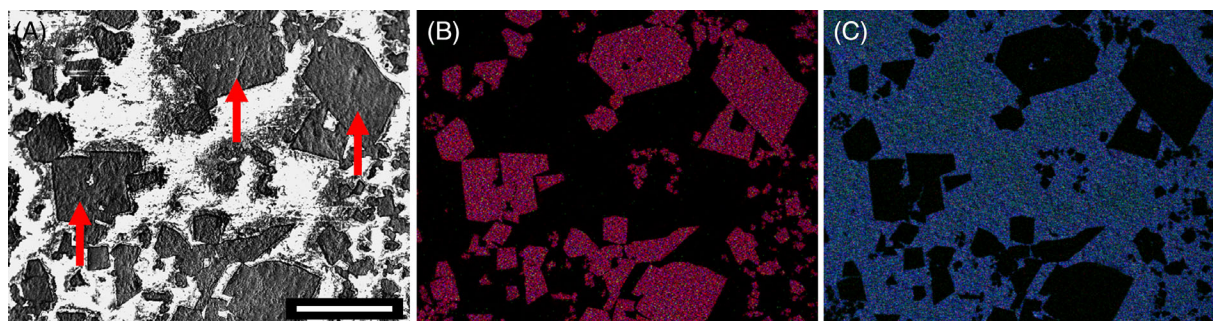


FIGURE 6 Spinel formation within the glass with a 200- μm scale bar: (A) secondary electron (SE) image with an arrow pointing at several $(\text{Ni},\text{Fe}^{2+})(\text{Cr},\text{Fe}^{3+})_2\text{O}_4$ spinels; (B) Fe represented as red, Ni as blue, and Cr as green, showing collocation of all these elements; (C) Al as red, Na as green, and Si as blue, showing collocation of all these elements

infiltration. This infiltration is interconnected in the refractory region as shown in Figure 4C, indicating a potential filling of grain boundaries or interconnected pores. Smaller, isolated infiltrations are found in the reaction region.

3.2 | Spinels

Spinels form both within the glass from its initial components and from refractory dissolution. A CPM (Figure 6) collected $\sim 12 \text{ mm}$ away from the melter wall suggests that the glass formed spinels also contain a small fraction of Cr. The glass was reported to have 0.16-wt% Cr_2O_3 ,¹⁴ whereas the Monofrax K-3 has a significant amount more Cr_2O_3 at 27.1 wt%,¹⁷ suggesting that the Cr found within spinels is due to the Cr leached out of the refractory. These spinels vary in size up to $\sim 200 \mu\text{m}$ in diameter.

A CPM collected near the refractory wall at the top of the RSM appears to contain two different phases, an

$(\text{Ni},\text{Fe}^{2+})(\text{Cr},\text{Fe}^{3+})_2\text{O}_4$ spinel and $(\text{Al},\text{Cr})_2\text{O}_3$ corundum phase, both indicated with arrows and labeled in Figure 7. It is likely that the refractory corundum phase breaks off into the melt, eventually dissolving into the melt, which is why it appears only near the refractory wall. Additionally, the spinels found near the RSM wall are $\sim 50 \mu\text{m}$ in diameter that is smaller than the spinels found away from the RSM wall.

Spinels formed within the glass of this RSM were reported by Matyáš et al.¹⁴ to be trevorite (NiFe_2O_4). For this study, multiple spinel locations (Figure 8) were measured with WDS and the element compositions are reported in Table 1. All the spinels are generally about the same composition, except for the spinels found at the top of the RSM adjacent to the boundary layer. At this location, there is a higher concentration of Al and lower concentration of Ni, compared to the other measured spinel compositions. It is possible that with forced convection, the glass (rich in Ni) had insufficient time to interact with the

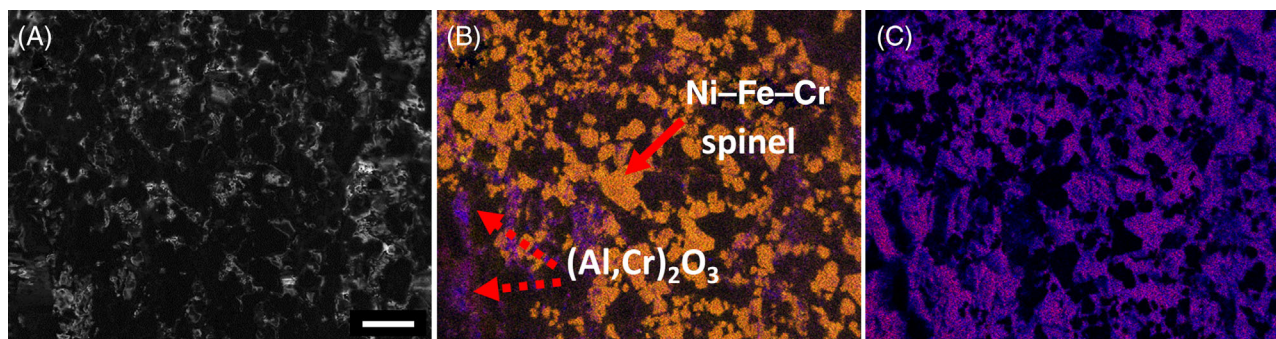


FIGURE 7 Spinel formation adjacent to the research-scale melter (RSM) wall with a 50- μm scale bar; (A) secondary electron (SE) image; (B) Fe represented as yellow, Ni as red, Cr as magenta, and Al as blue, showing the refractory phase $(\text{Al,Cr})_2\text{O}_3$ (indicated with a dashed arrow) floating amongst $(\text{Ni,Fe}^{2+})(\text{Cr,Fe}^{3+})_2\text{O}_4$ spinels (indicated with a solid arrow) within the melt; (C) Si as blue and Na as red, showing general colocation but not at the same concentrations, suggesting the glass phase

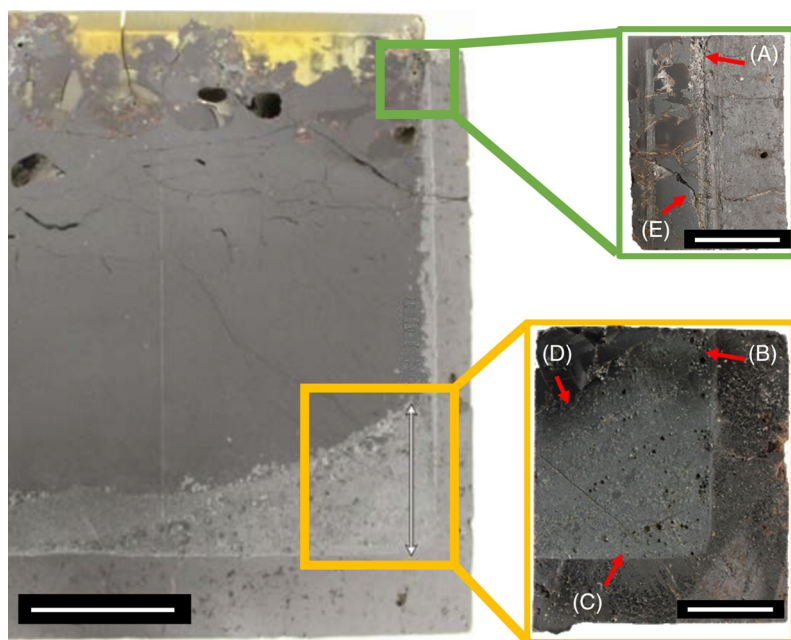


FIGURE 8 Locations of spinel measurements reported in Table 1. Locations A–C are spinels found adjacent to the reaction layer. Locations D and E are spinels found in the glass region. The cross-sectioned image of the research-scale melter (RSM) has a scale bar of 3.4 cm and the two images of the sample used in this study have a 1.27-cm scale bar. Partially modified from Ref. [14], used with permission courtesy of Battelle Memorial Institute

Monofrax K-3, resulting in higher measurements of Al (an element found within the refractory).

3.3 | Corrosion progression

A zonation map (Figure 9) of multiple elements reveals further insight into the layers of corrosion that occurred within this RSM. Each zonation map is specific to an element where a heat map describes the concentration of each element; the scale is from blue to red with increasing concentration. Figure 9 contains rough outlines of each observed section or layer (labeled 1–5) of corrosion. Beginning on the left in section 1, there is a high concentration of $(\text{Ni,Fe}^{2+})(\text{Cr,Fe}^{3+})_2\text{O}_4$ spinels within the glass. The reaction layer contains sections 2–4. The melt and reaction

layer interface in section 2 contains a high concentration of Fe and Ni, which is expected with a glass rich with both of these elements.¹⁴ In the reaction layer closer toward the refractory, section 3, there is a high concentration of Al leaching out of the refractory. Section 4 is the interface of the refractory and the reaction layer, where there is still evidence of elements from the glass (Ni,Fe) with the presence of refractory elements (Cr,Al,Mg). Finally in section 5, there is evidence of the two primary phases of Monofrax K-3, (I) $(\text{Al,Cr})_2\text{O}_3$ and (II) $(\text{Fe}^{2+},\text{Mg})(\text{Al,Cr})_2\text{O}_4$.

4 | DISCUSSION

As the glass melt encounters the refractory, an equilibrium between the solute (the glass melt) and the solvent

TABLE 1 Spinel elemental mol compositions at various locations (labeled A–E) throughout the research-scale melter (RSM)

Element	Spinel adjacent to the reaction layer			Spinel found in the glass	
	Top (A)	Mid (B)	Bottom (C)	Top (D)	Bottom (E)
Al ³⁺	0.22	0.03	0.02	0.03	0.04
Cr ³⁺	0.09	0.09	0.06	0.08	0.10
Fe ³⁺	1.70	1.89	1.91	1.89	1.86
Fe ²⁺	0.32	0.16	0.19	0.15	0.19
Ni ²⁺	0.67	0.83	0.79	0.84	0.79
Mg ²⁺	0.02	0.01	0.02	0.01	0.02

Note: Locations labeled below in Figure 8. Trivalent cations assumed to be in the spinel B site (sum = 2); Divalent cations assumed to be in the spinel A site (sum = 1).

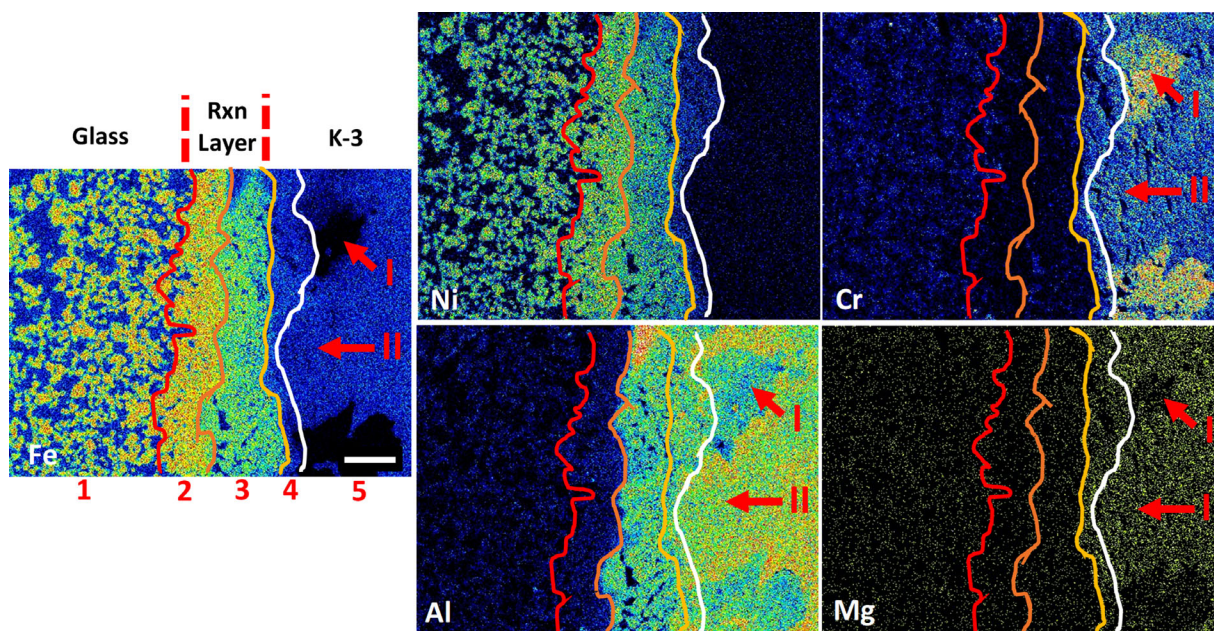


FIGURE 9 Zonation map showing the concentration of Fe, Ni, Cr, Al, and Mg. The sections of corrosion are outlined in each zonation map and labeled 1–5 under the Fe zonation map. The three main sections, glass, reaction (rxn) layer, and refractory are labeled above the Fe zonation map. The two primary phases of Monofrax K-3 are labeled (I) $(\text{Al,Cr})_2\text{O}_3$ and (II) $(\text{Fe}^{2+},\text{Mg})(\text{Al,Cr})_2\text{O}_4$. The scale bar is 100 μm .

(refractory) occurs. Indirect dissolution occurs and elements from the glass (Na,Si) infiltrate the refractory, whereas elements from the refractory (Al,Cr) leach out in the phase of $(\text{Al,Cr})_2\text{O}_3$ (the primary phase of Monofrax K-3). Further toward the base of the RSM, there is more evidence of Na infiltration into the refractory wall as discovered with CPMs. Within the same location containing increased Na infiltration, there is an increase in the thickness of the reaction layer. Both of these phenomena are due to the amount of physical erosion occurring; as the melt convection is less toward the base of the RSM, there is a thicker reaction layer protecting the corroded refractory (which contains Na from the melt) from spalling off into the melt.

At the top of the RSM, the forced convection causes the reaction layer to continuously separate and fall into the

melt, leaving the refractory exposed and in turn causing it also to corrode along grain boundaries and allow grains to spall off into the melt. In other words, the passivating reaction layer is continuously removed, exposing fresh refractory for further corrosion and chemical conversion into a reaction layer. The continuous removal of corroded refractory shows as a lack of Na infiltration near the top of the RSM. Further down into the RSM, the forced convection has less of an effect on the reaction layer, allowing it to build up in thickness and provide a passivation effect. This boundary protects the refractory from spalling off into the melt and is the reason why the corroded refractory is visible in the CPM (Figure 3).

Metal ions, such as Fe^{2+} , Fe^{3+} , and Ni^{2+} from the melt, react with the Cr^{3+} from the refractory to form the spinel interface layer at the leached refractory

boundary. Adjacent to the RSM at the top of the melter, there is evidence of corundum $(\text{Al,Cr})_2\text{O}_3$ interspersed with $(\text{Ni,Fe}^{2+})(\text{Cr,Fe}^{3+})_2\text{O}_4$ spinels in the quenched melt. This is due to forced convection causing exposed refractory to disintegrate and fall into the melt. Farther away from the refractory wall, there is evidence of only $(\text{Ni,Fe}^{2+})(\text{Cr,Fe}^{3+})_2\text{O}_4$ spinels suggesting the dissolution of the $(\text{Al,Cr})_2\text{O}_3$ corundum phase into the melt.

The full progression of corrosion was visible in Figure 9, which contained five main sections as labeled within the figure. The zonation maps show a high concentration of both Ni and Fe within section 1, which are the $(\text{Ni,Fe}^{2+})(\text{Cr,Fe}^{3+})_2\text{O}_4$ spinels. The reaction layer is shown in sections 2–4, which shows the process of equilibrium occurring between the melt and the refractory. Elements from the melt (Ni,Fe) diffuse toward the refractory, whereas elements from the refractory (Al,Cr) diffuse toward the melt. Section 5 shows the location of the two primary phases of Monofrax K-3, $(\text{Al,Cr})_2\text{O}_3$ and $(\text{Fe}^{2+},\text{Mg})(\text{Al,Cr})_2\text{O}_4$.

5 | CONCLUSION

This study investigated the corrosion of Monofrax K-3 refractory and the resulting microstructure obtained from an 11-week experiment melting an Fe- and Ni-containing borosilicate glass simulating a high-level nuclear waste vitrification process. CPMs showed elements from the melt (i.e., Ni,Fe) and the refractory (i.e., Cr) combined to create a reaction layer of $(\text{Ni,Fe}^{2+})(\text{Cr,Fe}^{3+})_2\text{O}_4$ spinels, which were readily found within the melt. Corundum $(\text{Al,Cr})_2\text{O}_3$, the primary phase of Monofrax K-3, was only found near the top of the RSM and adjacent to the melter wall, likely present due to the spallation of the refractory due to convection within the melter. The lack of $(\text{Al,Cr})_2\text{O}_3$ in other locations of the melter suggests it dissolved into the melt. Further down into the melt, the lack of forced convection compared to near the melt surface caused the reaction layer thickness to increase. The reaction layer can prevent melt infiltration into the refractory. Near the top of the RSM, the reaction layer thickness is relatively small due to the forced convection removing the spinels which the reaction layer comprises. This allows more refractory to become exposed to the melt. Deeper into the RSM, the reaction layer is thicker due to the reduced melt convection, creating a protective layer to the refractory.

ACKNOWLEDGMENTS

This research was performed with funding from the United States Department of Energy (US DOE) Office of Environ-

mental Management through the US DOE Waste Treatment & Immobilization Plant (WTP) Federal Project Office under the direction of Dr. Albert A. Kruger, contract numbers 89304017CEM000001 and 89304022CEM000015. The authors acknowledge Josef Matyáš and Will Eaton for graciously allowing their RSM to be the subject of this study. The authors thank Sam Karcher for his assistance with the field emission scanning electron microscope (FESEM). The WSU X-ray nano-computed tomography user facility was supported by the Joint Center for Research in Earth Abundant Materials (JCDREAM) and the Murdock Charitable Trust. The authors acknowledge the GeoAnalytical Laboratory at WSU for their use of the JEOL JXA-8500F field emission electron microprobe. Finally, the authors thank Raine Antonio for sample polishing and preparation for characterization.

REFERENCES

- Bingham PA, Connelly AJ, Hyatt NC, Hand RJ. Corrosion of glass contact refractories for the vitrification of radioactive wastes: a review. *Int Mater Rev*. 2011;56(4):226–42.
- Kwong K, Petty A, Bennett J, Krabbe R, Thomas H. Wear mechanisms of chromia refractories in slagging gasifiers: wear mechanisms of chromia refractories. *Int J Appl Ceram Technol*. 2007;4(6):503–13.
- Pecoraro GA. How the properties of glass melts influence the dissolution of refractory materials. *Properties of glass-forming melts*. *Advances in Fusion and Processing of Glass III*, Ceramic Transactions Vol 141. England: Taylor & Francis; 2005. p. 339–89.
- Lee WE, Zhang S. Melt corrosion of oxide and oxide-carbon refractories. *Int Mater Rev*. 1999;44(3):77–104.
- Iverson D, Imrich K, Bickford D, Gee J, Jenkins C, Heckendorn F. Examination of DWPF melter materials after 8 years of service. United States: Savannah River Site (SRS); 2003. WSRC-MS-2003-00318.
- Fox KM, Hodges BC, Imrich KJ, Iverson DC, Owen JE. Visual inspection of defense waste processing facility melter 2 interior after end of service. United States: Savannah River Site (SRS); 2018. SRNL-STI-2017-00428.
- Hubert M. Industrial glass processing and fabrication. In: *Musgraves JD, Hu J, Calvez L, editors. Springer handbook of glass*. Switzerland: Springer Nature; 2019. p. 1193–229.
- Lu XD, Gan H, Buechele AC, Pegg IL. Corrosion of K-3 glass-contact refractory in sodium-rich aluminosilicate melts. *MRS Proc*. 1998;556:279.
- Jantzen CM, Imrich KJ, Pickett JB, Brown KG. High chrome refractory characterization: Part II. Accumulation of spinel corrosion deposits in radioactive waste glass melters. *Int J Appl Glass Sci*. 2015;6(2):158–71.
- Soltan AM, Pöllmann H, Kaden R, König A, Abd EL-Raouf F, Eltaher M, et al. Degradation of aluminosilicate refractories: an integrated approach. *J Eur Ceram Soc*. 2015;35(16):4573–92.
- Riley BJ, Hrma P, Crum JV, Vienna JD, Schweiger MJ, Rodriguez CP, et al. Liquidus temperature in the spinel primary phase field: a comparison between optical and crystal fraction methods. *J Non-Cryst Solids*. 2018;483:1–9.

12. Matyáš J, Gervasio V, Sannoh SE, Kruger AA. Predictive modeling of crystal accumulation in high-level waste glass melter processing radioactive waste. *J Nucl Mater.* 2017;495:322–31.
13. Hrma P, Riley BJ, Crum JV, Matyáš J. The effect of high-level waste glass composition on spinel liquidus temperature. *J Non-Cryst Solids.* 2014;384:32–40.
14. Matyáš J, Sevigny G, Venarsky J, David J, Lukins C, Lang J, et al. Evaluation of crystal accumulation in high-level waste glasses with a research-scale melter. United States: Pacific Northwest National Laboratory; 2018. PNNL-27419.
15. Kingery WD. Kinetics of high-temperature processes. In: Kingery WD, editor. Cambridge: Technology Press of Massachusetts Institute of Technology; 1959.
16. Gan H, Lu X, Vidensky I, Paul MC, Pegg IL. Corrosion of K-3 refractory and metal alloys in RPP-WTP LAW glasses. United States: Vitreous State Laboratory; 2001. VSL-01R3540-1.
17. Jantzen CM, Imrich KJ, Brown KG, Pickett JB. High chrome refractory characterization: Part I. Impact of melt reduction/oxidation on the corrosion mechanism. *Int J Appl Glass Sci.* 2015;6(2):137–57.
18. Bennett JP, Kwong K-S. Failure mechanisms in high chrome oxide gasifier refractories. *Metall Mater Trans A: Phys Metall Mater Sci.* 2011;42(4):888–904.
19. Sandhage KH, Yurek GJ. Indirect dissolution of sapphire into silicate melts. *J Am Ceram Soc.* 1988;71(6):478–89.
20. Liu J, Guo M, Jones PT, Verhaeghe F, Blanpain B, Wollants P. In situ observation of the direct and indirect dissolution of MgO particles in CaO–Al₂O₃–SiO₂-based slags. *J Eur Ceram Soc.* 2007;27(4):1961–72.
21. Lee WE, Zhang S, Sarpoolaky H, Smith JD, Bennett JP. Different types of in situ refractories. In: Fundamentals of refractory technology. Ceramic Transactions Vol 125. American Ceramic Society. 2006. p. 245–52.
22. Selkregg K. Fusion cast refractories: roles of containment. *Am Ceram Soc Bull.* 2018;97:21–8.
23. Matyáš J, Vienna JD, Kimura A, Schaible MJ, Tate RM. Development of crystal-tolerant waste glasses. United States: Pacific Northwest National Laboratory; 2010. PNNL-20072.
24. Gan H, Lu X, Buechele AC, Paul MC, Pegg IL. Corrosion of chromium-rich oxide refractories in molten waste glasses. United States: Catholic University of America; 2002. DOE/ID/13587.
25. Probe Software Inc. Probe for EPMA. Eugene, OR: Probe Software Inc; 2005.

SUPPORTING INFORMATION

Additional supporting information can be found online in the Supporting Information section at the end of this article.

How to cite this article: Smith-Gray N, Bussey J, McCloy J. Microstructural examination of interactions between chromia-based refractory and nuclear glass in a melter. *J Am Ceram Soc.* 2022;105:7760–7769.
<https://doi.org/10.1111/jace.18706>